

See discussions, stats, and author profiles for this publication at: <https://www.researchgate.net/publication/275208632>

New Insights into Corrosion of Ruthenium and Ruthenium Oxide Nanoparticles in Acidic Media

ARTICLE *in* THE JOURNAL OF PHYSICAL CHEMISTRY C · APRIL 2015

Impact Factor: 4.77 · DOI: 10.1021/acs.jpcc.5b01832

CITATIONS

2

READS

101

10 AUTHORS, INCLUDING:



[Nejc Hodnik](#)

Max Planck Institute for Iron Research GmbH

40 PUBLICATIONS 128 CITATIONS

[SEE PROFILE](#)



[Milena Zorko](#)

National Institute of Chemistry

35 PUBLICATIONS 181 CITATIONS

[SEE PROFILE](#)



[Vid Simon Šelih](#)

National Institute of Chemistry

25 PUBLICATIONS 381 CITATIONS

[SEE PROFILE](#)



[Miran Gaberscek](#)

National Institute of Chemistry

181 PUBLICATIONS 4,604 CITATIONS

[SEE PROFILE](#)

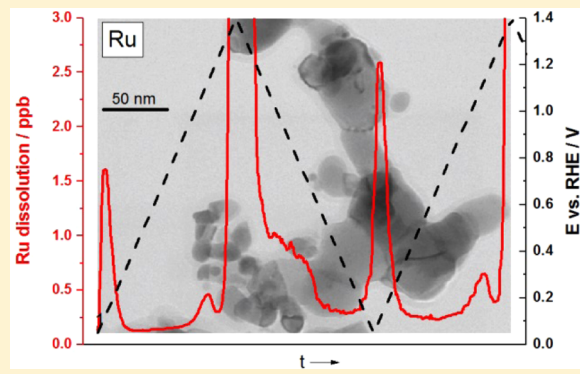
New Insights into Corrosion of Ruthenium and Ruthenium Oxide Nanoparticles in Acidic Media

Nejc Hodnik,^{*,†,§} Primož Jovanovič,[†] Andraž Pavlišič,[†] Barbara Jozinovič,[†] Milena Zorko,[†] Marjan Bele,[†] Vid Simon Šelih,[‡] Martin Šala,[‡] Samo Hočevar,[‡] and Miran Gaberšček^{*,‡}

[†]Laboratory for Materials Chemistry and [‡]Analytical Chemistry Laboratory, National Institute of Chemistry, Hajdrihova 19, 1000 Ljubljana, Slovenia

Supporting Information

ABSTRACT: The dissolution behaviors of Ru and ruthenium oxide nanoparticles in acidic media were studied for the first time using highly sensitive *in situ* measurements of concentration by inductively coupled plasma mass spectrometry (ICP-MS). Online time- and potential-resolved electrochemical dissolution profiles revealed novel corrosion features (signals) in the potential window from 0 to ~ 1.4 V, where known severe dissolution due to the oxygen evolution reaction (OER) takes place. Most of the features follow the thermodynamic changes of the Ru oxidation/reduction state, which consequently trigger so-called transient dissolution. An as-synthesized Ru sample was found to exhibit an order-of-magnitude higher dissolution rate than an electrochemically oxidized amorphous Ru sample. The latter, in turn, dissolved about 10 times faster than rutile RuO₂. The observed OER activity was in an inverse relationship with the measured dissolution. Disagreement was found with the general assumption that the onset of the OER should coincide with the onset of Ru dissolution. Interestingly, in all samples, Ru dissolution was observed at about 0.17 V lower potentials than the OER. The present results are relevant for various energy-conversion and -storage devices such as proton-exchange membrane electrolyzers, low-temperature fuel cells, reverse fuel cells, supercapacitors, batteries, and photocatalysts that can contain Ru as an active component.



1. INTRODUCTION

Ruthenium-based materials are well-known for their catalytic properties in many heterogeneous and homogeneous catalytic reactions.¹ In light of recent increasing demands for reduced CO₂ emissions and sustainable energy,^{2,3} ruthenium can be recognized as a very important element. For example, ruthenium is used in the anodes and cathodes of proton-exchange membrane (PEM) electrocatalytic reactors such as electrolyzers, fuel cells, and reverse fuel cells.^{2–5} Ru has been reported to promote reactions such as hydrogen oxidation and evolution,^{6,7} carbon monoxide oxidation,⁸ methanol oxidation,^{9–12} oxygen reduction^{13,14} and oxygen evolution.^{2,15–30} The past several years have witnessed a renewed interest in PEM electrolyzer technology, as it offers very elegant ways to utilize energy coming from dynamic electrical sources such as wind turbines and solar cells. Additionally, PEM electrolyzers can greatly benefit from the in-depth knowledge gained during the intense research into PEM fuel cells, where identical fundamental issues have been tackled for many years. It seems that selected problems such as lowering the noble-metal content or improving the catalyst stability can be addressed based on the same materials concepts, for instance, core–shell catalyst structures. Interestingly, RuO₂ can also be used for carbon corrosion protection to extend the performance of the

electrocatalysts used in PEM fuel cells³¹ or even as a substitute for carbon as a support.³² Further important applications of RuO₂ can be found in supercapacitors,^{33–37} transparent conducting films,³⁸ photocatalysts,³⁹ and batteries.³⁶ Therefore, studying fundamental processes of ruthenium dissolution is a very important direction to be pursued in the search for more stable energy conversion and storage materials. This could have an especially significant effect on the development of novel, more stable catalysts, as well as on the determination of optimal operating conditions for PEM fuel cells and electrolyzers.²

Until now, highly accurate studies involving potential-resolved dissolution profiles have been carried out on only polycrystalline Ru and Ru-based dimensionally stable anodes (DSAs).^{23,30} The most promising material in terms of its activity in the oxygen evolution reaction (OER) is ruthenium oxide,^{2,15,21,23,30} which is also used in the chlor-alkali industry.²⁰ Ruthenium oxide has versatile oxidation properties because of its complex and unique redox surface chemistry behavior.^{1,40} However, the main drawback is its poor stability.^{2,20,23,25,26,30} In terms of the industrial application of electrolyzers, major

Received: February 24, 2015

Revised: April 8, 2015

progress was made by the introduction of dimensionally stable anodes (DSAs), which still provide a state-of-the-art solution to the corrosion issues of Ru-based catalysts.^{15,16} In general, it is known that thermally prepared ruthenium dioxide (th. RuO₂, with a rutile crystal structure) is more stable against dissolution than electrochemically prepared ruthenium oxide (el. RuO₂, with an amorphous crystal structure) (th. RuO₂ > el. RuO₂).^{17,18,22,25–28} Interestingly, the OER activities of these materials exhibit the opposite order (el. RuO₂ > th. RuO₂).^{18,22,25,27,28} This is in line with the general belief that OER activity and stability are in an inverse relationship,^{24,26,29,41} where the onset of the OER should coincide with Ru corrosion.^{17,18,29} However, at least two recent reports do not support this “rule” by clearly showing that activity and stability are not necessarily in a tradeoff correlation.^{25,30}

For the first time, extremely sensitive time- and potential-resolved inductively coupled plasma mass spectrometry (ICP-MS) electrochemical dissolution profiles of three different types of ruthenium oxide nanoparticles, namely, as-synthesized Ru and electrochemically and thermally prepared RuO₂, are presented. We clearly observed multiple Ru dissolution features for all samples in the whole potential range from 0 V to the OER operating conditions (1.4 V vs RHE), where massive dissolution occurred. Not only was a much more accurate method used, but the potential range was also significantly extended with respect to most other reports in which Ru dissolution was primarily studied below 0.5 V and above 1.23 V vs RHE.^{23,30} We show that the amount and the shape of the dissolution profiles are highly dependent on the preparation^{17,18,22,25–28} and pretreatment²⁷ of the Ru sample. Online ICP-MS dissolution data were supported by thin-film rotating-disk electrode (TF-RDE) and identical-location scanning electron microscopy (IL-SEM) results.

2. EXPERIMENTAL SECTION

RuO₂ was prepared by dissolving 0.3 mmol of Ru salt (ruthenium chloride; Acros Organics, Geel, Belgium) and 0.3 mmol of citric acid (Sigma-Aldrich, St. Louis, MO) in 5 mL of water. The solution was mixed at 50 °C until evaporation. Afterward, the mixture was thermally treated at 500 °C in an air atmosphere for 5 h. At this point, most of the carbon was burned away, as can be seen from TEM images (Supporting Information, Figures S1 and S2). Pure metallic Ru was prepared by reducing the RuO₂ in a furnace at 500 °C under a reductive hydrogen atmosphere (5% H₂ in Ar) for 5 h. Therefore, we assumed that we had, in principle, a similar particle size distribution profile with a systematic decrease in size for metallic Ru due to absence of oxygen in the crystal structure. El. RuO₂ was prepared by irreversibly electrochemically oxidizing Ru sample with 200 potential cycles between 0.05 and 1.2 V.

An electrochemical flow cell (EFC) coupled with an ICP-MS setup was already introduced in our previous publications.^{42,43} In brief, a commercial BASi electrochemical flow cell (Cross-Flow Cell Kit MW-5052) with a homemade silicon gasket of 1-mm thickness was coupled with an Agilent 7500ce ICP-MS instrument (Agilent Technologies, Palo Alto, CA) equipped with a MicroMist glass concentric nebulizer and a Peltier-cooled Scott-type double-pass quartz spray chamber. A forward radio-frequency power of 1500 W was used with Ar gas flows: carrier, 0.85 L/min; makeup, 0.28 L/min; plasma, 1 L/min; and cooling, 15 L/min. Perchloric acid (HClO₄; 0.1 mol/L, 70%, 99.999% trace metals basis; Aldrich) was used as the electrolyte carrier medium. Solutions were pumped at 263 μL/min using a

syringe pump (WPI sp100i). Catalyst thin-film preparation was the same as for the thin-film rotating-disk electrode (TF-RDE) measurements. Three milligrams of catalyst was dispersed in Milli-Q water. The suspension was drop cast on a glassy carbon electrode and stabilized with 5 μL of Nafion diluted in isopropanol (1:50). The amount of Ru deposited was 5 μg, whereas for el. RuO₂ and th. RuO₂, the amount was 10 μg. The experimental procedure involved consecutive cycling from 0.05 V to different upper potential limits starting at 0.4 V and increasing by 0.1 to 1.6 V vs RHE. Compared to electrochemical cyclovoltammetry measurements (TF-RDE and rotating ring-disk electrode) the online ICP-MS method provide a much higher accuracy when dissolution is studied.

At each potential, three cycles were recorded. The TF-RDE and IL-SEM experimental procedures were already explained in our previous articles.^{44,45} Electrochemical TF-RDE degradation was performed by executing 1000 cycles between 0.8 to 1.3 V vs SCE with a scan rate 1 V/s.

3. RESULTS AND DISCUSSION

X-ray powder diffraction of metallic Ru and th. RuO₂ revealed no overlapping diffraction peaks of the two samples, indicating two different crystal structures (Figure 1). The former was

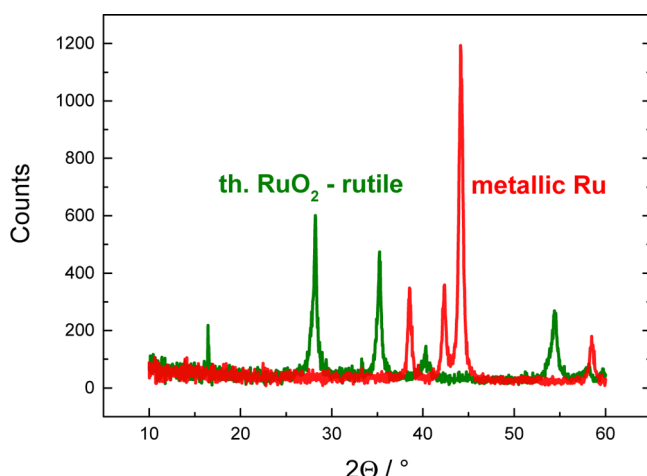


Figure 1. XRD spectra of metallic Ru and th. RuO₂ nanoparticles.

characteristic for pure metallic ruthenium, whereas the spectrum for th. RuO₂ sample was typical of the rutile crystal structure. The particle size distributions for the two samples were similar, ranging mainly from 5 to 100 nm. In addition, some larger particles with typical sizes up to almost 1 μm were observed (see TEM images in the Supporting Information, Figures S1 and S2).

Before analyzing the measured dissolution results, we note that, in noble metals, two essentially different types of dissolution events have been reported. Apart from the conventional thermodynamically driven instability occurring at well-defined potentials, there are increasingly many reports about degradation phenomena that are merely a consequence of a disturbance of the crystal structure related to a change in the oxidation state of the transition metal. For example, when oxygen atoms are inserted into or removed from the structure during oxidation/reduction, a dissolution event can occur. Hence, the term transient dissolution has been used when referring to this type of phenomenon.^{23,46} An existing working hypothesis explaining transient dissolution is as follows: Either

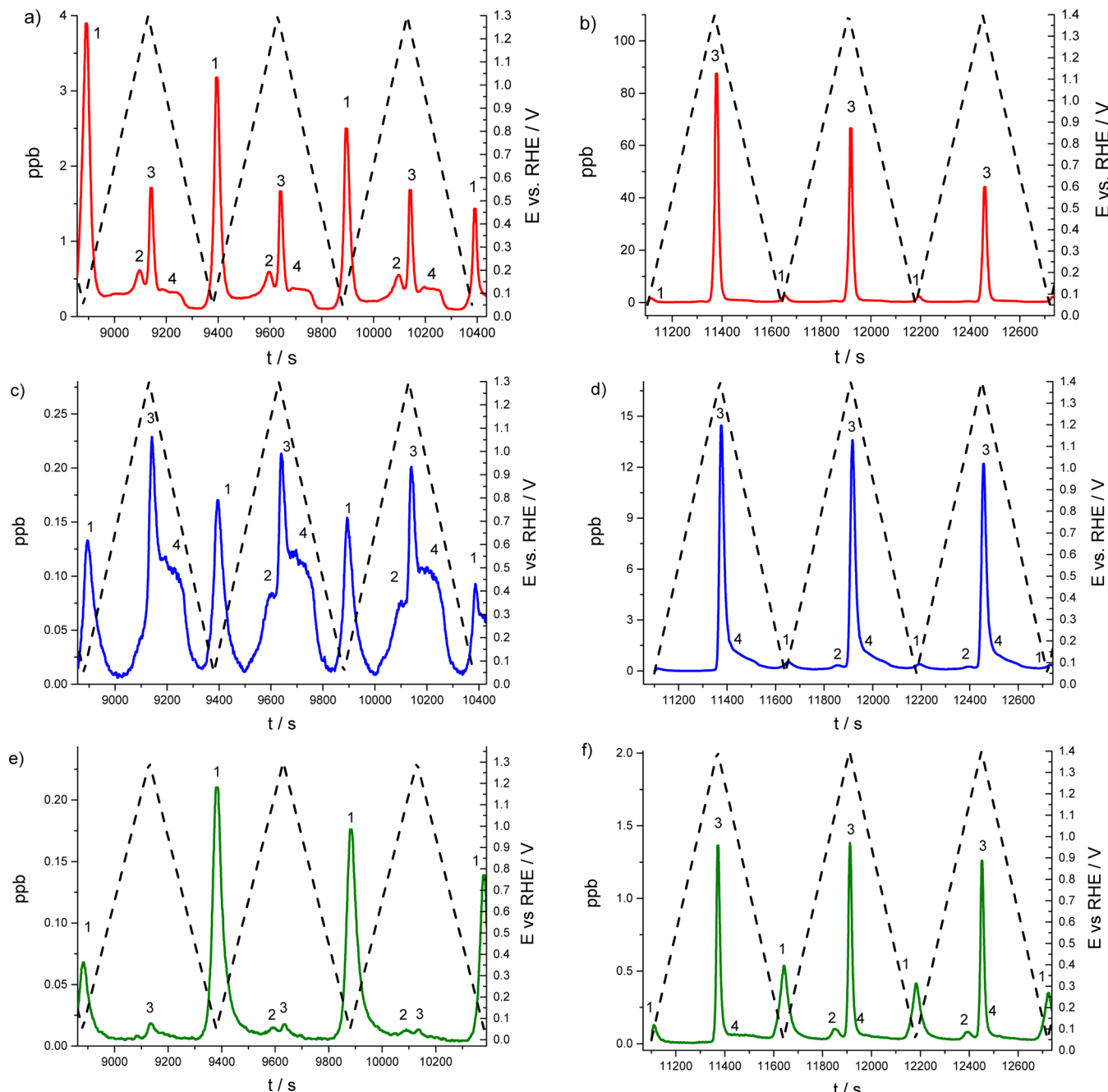


Figure 2. Potential-resolved ruthenium electrochemical dissolution of as-synthesized Ru (red), el. RuO₂ (blue), and th. RuO₂ (green) nanoparticles with upper potential limits of 1.3 V (left column) and 1.4 V (right column) vs RHE in 0.1 M HClO₄ at a sweep rate of 5 mV/s. Solid curves represent the concentration of dissolved Ru (left ordinate axes), whereas dashed curves show the corresponding potentials (right ordinate axes).

a low coordination site or a metastable transition state becomes exposed to the electrolyte and subsequently dissolves away^{23,42,46,47} or is even simply ejected from the structure. In the case of Ru, direct anodic dissolution is also possible above ca. 0.5 V,^{40,48} if metallic Ru is exposed to the electrolyte as a result of the disturbance of surface oxidation/reduction (resembling formation of a crack).

The present high-accuracy experiments typically revealed four characteristic features (three peaks and a shoulder) in the Ru dissolution profiles for all three samples when cycled from 0.05 to 1.3 and 1.4 V vs RHE (see Figure 2 and the enlarged dissolution profile in Figure S3 of the Supporting Information). These degradation events can be assigned to different

transitions of Ru oxidation states,⁴⁸ as indicated in Table 1. More data on dissolution features of Ru and el. RuO₂ when cycled to 1 V are provided in the Supporting Information (Figure S2 and Table S1).

Note that as-synthesized Ru nanoparticles cannot be considered as pure metallic Ru because air exposure⁴⁹ and especially precycling already induce at least oxidation of the Ru surface.⁴⁸ This is in line with the observed initial cathodic dissolution (first peak 1 in Figure S3a, Supporting Information), which is a result of the reduction of “irreversible” RuO_x. Because there was no bare Ru surface, we did not observe any dissolution of Ru into Ru₂O₃ at 0.7 V or a direct electrochemical dissolution of Ru into Ru²⁺ at 0.45 V.⁴⁸ In

Table 1. Four Characteristic Features of Ru Electrochemical Dissolution as Observed in Figure 1 Are Associated with Selected Ruthenium Redox Processes Predicted by the Pourbaix Diagram^{48a}

peak	dissolution process	reaction	potential ^b or E
1	transient dissolution (reduction of “irreversible” RuO_x)	$\text{RuO}_x + 2x\text{H}^+ + 2x\text{e}^- = \text{Ru} + x\text{H}_2\text{O}$	0.2–0.05 V vs RHE
2	transient dissolution (oxidation)	$\text{Ru}_2\text{O}_3 + \text{H}_2\text{O} = 2\text{RuO}_2 + 2\text{H}^+ + 2\text{e}^-$	0.937 V – 0.0591pH
3	anodic oxidation with subsequent chemical dissolution or direct anodic dissolution (oxidation)	$\text{RuO}_2 + 2\text{H}_2\text{O} = \text{RuO}_4 + 4\text{H}^+ + 4\text{e}^-$ $\text{RuO}_4 + \text{H}_2\text{O} = \text{H}_2\text{RuO}_5(\text{aq})$	1.387 V – 0.0591pH
4	transient dissolution (reduction of “reversible” RuO_x) with subsequent direct anodic dissolution	$\text{RuO}_2 + 3\text{H}_2\text{O} = \text{H}_2\text{RuO}_5(\text{aq}) + 4\text{H}^+ + 4\text{e}^-$ $2\text{RuO}_2 + 2\text{H}^+ + 2\text{e}^- = \text{Ru}_2\text{O}_3 + \text{H}_2\text{O}$ $\text{Ru}_2\text{O}_3 + 6\text{H}^+ + 6\text{e}^- = 2\text{Ru} + 3\text{H}_2\text{O}$ $\text{Ru} = \text{Ru}^{2+} + 2\text{e}^-$	1.400 V – 0.0591pH + 0.0148 log $[\text{H}_2\text{RuO}_3]$ 0.937 V – 0.0591pH 0.738 V – 0.0591pH 0.455 V + 0.0295 log $[\text{Ru}^{2+}]$

^aTable does not necessarily include all possible dissolution scenarios for the present Ru-based samples. ^bPotentials given with respect to the normal hydrogen electrode (NHE), unless stated otherwise.

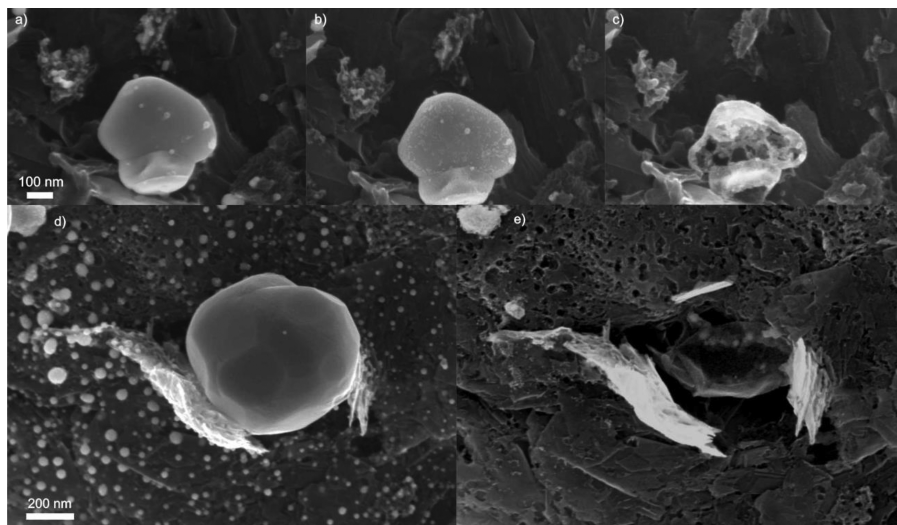


Figure 3. (a–c) IL-SEM images of as-prepared Ru (a) before cycling and after the (b) first and (c) second cycles from 0.05 to 1.6 V vs RHE. (d,e) IL-SEM images of (d) as-prepared Ru and (e) Ru after 10 cycles from 0.05 to 1.6 V vs RHE.

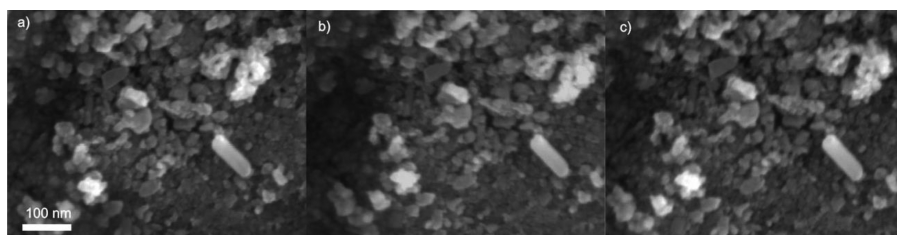


Figure 4. RuO_2 (a) before cycling, (b) after 10 cycles from 0.05 to 1.6 V vs RHE, and (c) after 10000 cycles from 1.18 to 1.58 V vs RHE.

other words, peak 4 was missing for our as-synthesized Ru when going in the anodic direction. In any case, the Ru sample revealed a different behavior depending on the electrochemical conditions. For example, when a fresh Ru sample was cycled only up to 1 V, we indeed observed features that could be ascribed to process 4 predicted in Table 1 (see peaks 5–7 in Figure S4, Supporting Information). However, when fresh (pure) Ru was exposed to a few excursions above 1 V, it was irreversibly oxidized. This electrochemically formed ruthenium oxide, also referred to as hydrous $\text{RuO}_2 \cdot x\text{H}_2\text{O}$, was amorphous and porous and contained a lot of defects and water.^{1,26,50} When pure ruthenium nanoparticles were cycled to potentials as high as 1.6 V vs RHE, a severe degradation due to ruthenium dissolution and the complete dissolution of small particles after 10 cycles (Figure 3 and Figure S5, Supporting Information)

were observed. Note that the large particle in Figure 3d and another one in Figure S5a (Supporting Information) were detached during the cycling. Interestingly, the complete dissolution of Ru nanoparticles with a crystallite size of around 5 nm was previously observed already after first anodic scan in an excursion above 1.4 V.²¹ Here, however, we observed a severe degradation in the first 90 degradation cycles followed by complete dissolution after 1000 degradation cycles from 1.18 to 1.58 V vs RHE (Figures S6 and S7, Supporting Information). The reason for this discrepancy might be the incomplete reduction of our sample to metallic Ru during the synthesis. As a result, some oxidized Ru, which, as shown below, is more stable, might have been left in the final product.

When oxide was prepared by a thermal treatment as part of the synthesis, it was more packed (rutile crystal type) and more

stable.^{25,26} It can be clearly seen from Figure 4 that the morphology of th. RuO₂ did not change even after prolonged degradation (10000 cycles) and that its activity was not dramatically lowered (Figures S6 and S7, Supporting Information). This degradation probably occurred only on the surface of th. RuO₂ and was therefore not observed in the relatively low-resolution IL-SEM images (Figure 4).

Interestingly, all samples exhibited a cathodic dissolution peak at a negative cycle potential limit (peak 1 appearing slightly below 0.2 V; see Figure 2), which was probably due to the partial reduction of the irreversibly formed ruthenium oxide. In their studies,⁷ Kötz and Stucki concluded that, under hydrogen-evolution conditions, RuO₂ was only partially reduced and metallic Ru did not form. A closer inspection of a recent work by Cherevko et al.²³ also revealed a small ruthenium dissolution peak at negative potentials. Zeradjanin et al.³⁰ observed a severe cathodic dissolution during a cathodic excursion starting below 0.5 V. According to their interpretation, this reaction corresponds to the redox transition from RuO₂ to Ru³⁺.⁴⁰ Indeed, we also observed a peak at the same potential (peak 7 in Figure S4a, Supporting Information); however, it was clearly separated from feature 1 and was observed only in the pure Ru sample when cycled up to a potential limit of 1 V. Another feature, less dominant but clearly resolved in the cathodic scans of all samples, is the shoulder denoted as feature 4 in Figure 2 (see also Figure S3, Supporting Information). This shoulder can be associated with the reduction of any type of ruthenium oxide (for instance, Ru₂O₃ and RuO₂, as indicated in Table 1), as well as with a reaction of bare (pure) Ru underneath the oxides. Possible further dissolution reactions can be found in the Supporting Information.

Close inspection of Figure 2 reveals that, in el. RuO₂ and th. RuO₂, the dissolution peak at approximately 0.9 V (peak 2; see also zoomed measurements in Figure S3a–d, Supporting Information) related to the oxidation of Ru₂O₃ to RuO₂ was very small or probably even completely absent during the first cycle. This is presumably because Ru₂O₃ had not formed yet. The peak appeared only when the RuO₂ crystal structure was appropriately perturbed, for example, when exposed to the OER process. Already 1.3 V was sufficient for small feature 2 to appear (see left columns of Figure 2). When going to 1.4 V, however, this feature was already well expressed in both el. and th. RuO₂ (Figure 2 and Figure S3, Supporting Information). We assume that this is because a full sequence of reactions corresponding to peaks 3 and 4 is needed for Ru₂O₃ to be formed from RuO₂.

The nature of peak 3 shown in Figures 2 and 5 is elusive, and we propose two tentative explanations in Table 1. The most obvious one is the well-known process that is directly coupled with OER of RuO₂ oxidation to RuO₄ (1.387 V – 0.0591pH); the latter is highly unstable and subsequently decomposes back to RuO₂ and O₂. On the other hand, it is clear that the onset of this peak coincides with the theoretical potential of the OER, that is, 1.23 V (Figure 5), as already observed in a recent report by Zeradjanin et al.³⁰ A second option to be considered is the direct anodic dissolution of RuO₂ to soluble H₂RuO₅ (1.400 V – 0.0591pH + 0.0148 log [H₂RuO₅]). Taking into account the pH term (0.1 M HClO₄), we obtain a potential of 1.3409 V. When additionally subtracting the Nernstian part (i.e., 0.0148 log [H₂RuO₅]), a further downshift of approximately 100 mV could indeed be possible, provided that the H₂RuO₅(aq) concentrations are in the range of 10⁻⁷ M. On

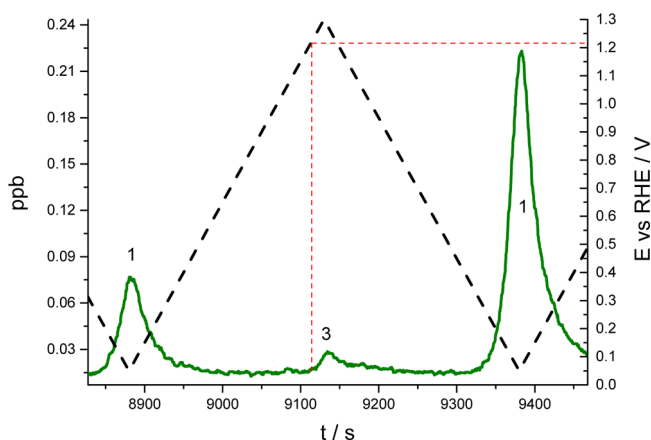


Figure 5. Potential-resolved ruthenium electrochemical dissolution of th. RuO₂ nanoparticles with an upper potential limit of 1.3 V vs RHE in 0.1 M HClO₄ at a sweep rate of 5 mV/s.

the other hand, the real onset of the OER potential in an electrolyzer, also referred to as the thermoneutral voltage, is about 0.25 V higher than the theoretical equilibrium voltage (at room temperature).⁵¹ We observed such an onset just below 1.4 V (Figure S8, Supporting Information), which is in accordance with the literature.^{18,23,24,26,27} Thus, quite unexpectedly, a noticeable corrosion occurred already at 1.23 V, that is, about 0.17 V lower than the onset of the OER. This is in disagreement with the general assumption that the onset of the OER coincides with the onset of Ru dissolution.^{17,18,29} However, the different points of onset of these processes do not necessarily mean that they proceed independently also at higher potentials (OER current densities). Interestingly, closer inspection of the figures in a recent iridium stability study⁵² revealed that some nanostructured iridium oxide samples also exhibited dissolution below the OER onset potentials.

The much-enhanced corrosion above ca. 1.4 V, observed in all of our samples (Figure 2), is in accordance with the reaction at 1.387 V – 0.0591pH predicted by the Pourbaix diagram.⁴⁸ This reaction corresponds to the formation of RuO₄ (feature 3 in Table 1 and Figure 2), which is an unstable compound, soluble in water and sometimes even considered an intermediate in the OER^{2,18,23} because it can decompose to O₂ and RuO₂.¹⁷ This is the background of the hypothesis claiming that stability is directly coupled with activity.^{25,26} Interestingly, Cherevko et al. interrelated the OER Tafel slope and the stability of noble metals, where, for Ru, the Tafel slope was small and the dissolution rate was high.²³ However, as mentioned before, this dissolution can also be theoretically interpreted as a direct anodic dissolution. Earlier studies using XPS by Kötz et al. and isotope labeling by Wohlfahrt-Mehrens et al. pointed to a ruthenium oxide-mediated OER mechanism, namely, an anodic oxidation with subsequent chemical dissolution.^{17,18,23} Unfortunately, using the present setup, it was not possible to distinguish between these two processes. In any case, it seems very likely that dissolution starts at 1.23 V through direct anodic dissolution. Then, somewhere between 1.3 and 1.4 V, the formation of unstable RuO₄ together with OER sets in. Finally, our results confirmed the previously observed inverse relationship between activities (Figures S6–S8, Supporting Information) and stabilities (Figure 2 and Table S2, Supporting Information).

In contrast to previous reports based on potential-resolved Ru dissolution profiles,^{23,30} we clearly observe dissolution

features at potentials between 0.5 and 1.23 V (Figure S4, Supporting Information). Even in the case of th. RuO₂, we saw a dissolution process occurring between 0.95 and 1 V (peak 2 in Table 1). However, the dissolved amounts were very small. Therefore, th. RuO₂ indeed seemed to be stable in the potential window from 0.2 to 1.3 V. For Ru, and also for el. RuO₂, multiple features could be seen even at lower potentials (Figure S4 and Table S1, Supporting Information). In previous studies, these features were probably masked by massive OER-induced corrosion.

Interestingly, when going to 1.4 V, all samples exhibited comparable amounts of cathodically dissolved Ru associated with peak 1. However, at the upper potential of 1 V, the th. RuO₂ sample exhibited order-of-magnitude lower dissolution amounts compared to the other samples. This is more evidence, although indirect, that the disturbance of the rutile crystal structure at 1.4 V induced irreversible effects such as the formation of less stable Ru₂O₃. For precise amounts of dissolved ruthenium, see Table S2 (Supporting Information). One of the reasons for the higher Ru dissolution from Ru and el. RuO₂, as compared to th. RuO₂, under OER conditions is also the formation of porous hydrous oxide (see Figure 3c and Figures S5c and S9, Supporting Information) and therefore the higher void fraction of the nanoparticles.^{2,16,17,25,26,50} However, this difference is probably not large enough to explain an order-of-magnitude higher dissolution rate.

Overall, it was found that thermally prepared RuO₂ with the rutile crystal structure exhibited an order-of-magnitude higher electrochemical stability (that is, a lower dissolution rate) in the whole potential range compared to electrochemically prepared RuO₂ and especially with respect to Ru (Table S2, Supporting Information). The higher stability is probably due to the higher crystallinity with many fewer defects compared to the electrochemically prepared porous hydrous RuO₂^{25,26} impeding the change of Ru(IV) oxidation state. As expected, the metallic Ru sample was found to be the most unstable. In this case, particles smaller than about 100 nm completely dissolved within first 10 cycles (Figure 2d,e), and after 90 cycles, the activity was almost completely lost (Figure S7, Supporting Information). The presence of large particles was probably the main reason that Ru seemed more stable in our measurements than in the study by Reier et al.,²¹ who used quite uniform 5-nm particles. The dissolution trend for the three samples used in the present study was as follows: Using the potential limit of 1.4 V, the amount of dissolved Ru was about 10 times larger than the amount of dissolved el. RuO₂ and about 100 times larger than the amount of dissolved th. RuO₂. Interestingly, the fraction of dissolved Ru per cycle in the present Ru and el. RuO₂ samples was within the same order of magnitude as found previously for 3- and 30-nm Pt nanoparticles.^{42,43}

4. CONCLUSIONS

For the first time, online potential- and time-resolved ruthenium electrochemical dissolution profiles of three as-synthesized ruthenium-based nanoparticles in an acidic environment have been presented. We report on multiple Ru dissolution features found in metallic Ru as well as in electrochemically and thermally prepared RuO₂ nanoparticles in a wide potential range (0.05–1.4 V). Most of the features occurring between 0 and 1.23 V can be associated with transient dissolution rather than direct (thermodynamic) dissolution. This means that, whenever the ruthenium oxidation state in the solid is changed, Ru atoms are removed. In other

words, whenever oxygen atoms are inserted or deinserted from the native crystal, this perturbation induces the formation of low-coordinated, unstable Ru atoms that are highly prone to dissolution. Direct anodic dissolution peak at low potentials (0.45 V) was also observed in the as-synthesized Ru sample. El. RuO₂ displayed clear transient dissolution features below 1 V. By contrast, th. RuO₂ seemed to be stable in the potential window between 0.2 to 1.3 V, where the oxidation state of Ru(IV) is stabilized against any redox reaction. This factor should be considered in studying and designing electrocatalysts for potential use in PEM electrochemical reactions as well as in materials used in supercapacitors, batteries, and photocatalysts.

At potentials higher than that usually associated with the onset of the OER (approximately 1.4 V), all ruthenium samples showed massive dissolution. The as-synthesized Ru sample exhibited dissolution that was about 10 times faster than that of the electrochemically produced RuO₂ and about 100 times faster than that of the thermally produced RuO₂. Interestingly, the dissolution rates of Ru and el. RuO₂ were found to be in the same range as the dissolution rate of platinum nanoparticles having sizes of 3 and 30 nm.⁴² Our studies confirmed the previous finding that stability and activity are in an inverse relationship. However, we could not confirm another general hypothesis, namely, that the onset of the OER coincides with the onset of Ru dissolution. In our case, we observed dissolution at 1.23 V vs RHE, which was about 0.17 V lower than the OER onset.

We note here that the present study was focused on basic measurements using the EFC-ICP-MS setup in studying Ru dissolution mechanisms. A more comprehensive work on Ru-based materials of practical importance, in particular those forming mixed oxides with Ir, Pt, Sn, Rh, Cu, and so on,^{4,12} and on materials forming supports (such as Ti- or Ta-based oxides or carbides⁵) is in progress. Additionally, the present results open up interesting new questions that will be addressed in the future such as dissolution at constant potential, the effects of scan rate, and particle-size-dependent stability.

■ ASSOCIATED CONTENT

§ Supporting Information

Supplementary information about our samples including TEM images, additional potentials, and Ru dissolution profiles; IL-SEM image, TF-RDE degradation measurements, and electrochemical measurements obtained in an electrochemical flow cell. This material is available free of charge via the Internet at <http://pubs.acs.org>.

■ AUTHOR INFORMATION

Corresponding Authors

*E-mail: nejc.hodnik@ki.si.

*E-mail: miran.gaberscek@ki.si.

Present Address

[§]N.H. is currently at Max Planck Institut für Eisenforschung GmbH, Department of Interface Chemistry and Surface Engineering, Max-Planck-Strasse 1, 40237 Düsseldorf, Germany.

Author Contributions

The manuscript was written through contributions of all authors. All authors have given approval to the final version of the manuscript.

Notes

The authors declare no competing financial interest.

ACKNOWLEDGMENTS

Financial support from the Slovenian Research Agency is gratefully acknowledged. We acknowledge Dr. Karl Mayrhofer (Max Planck Institut für Eisenforschung GmbH) for TEM images.

REFERENCES

- (1) Over, H. Surface Chemistry of Ruthenium Dioxide in Heterogeneous Catalysis and Electrocatalysis: From Fundamental to Applied Research. *Chem. Rev.* **2012**, *112*, 3356–3426.
- (2) Katsounaros, I.; Cherevko, S.; Zeradjanin, A. R.; Mayrhofer, K. J. Oxygen Electrochemistry as a Cornerstone for Sustainable Energy Conversion. *Angew. Chem., Int. Ed.* **2014**, *53*, 102–121.
- (3) Greeley, J.; Markovic, N. M. The Road from Animal Electricity to Green Energy: Combining Experiment and Theory in Electrocatalysis. *Energy Environ. Sci.* **2012**, *5*, 9246–9256.
- (4) Chen, G.; Delafuente, D. A.; Sarangapani, S.; Mallouk, T. E. Combinatorial Discovery of Bifunctional Oxygen Reduction–Water Oxidation Electrocatalysts for Regenerative Fuel Cells. *Catal. Today* **2001**, *67*, 341–355.
- (5) Park, S.; Shao, Y.; Liu, J.; Wang, Y. Oxygen Electrocatalysts for Water Electrolyzers and Reversible Fuel Cells: Status and Perspective. *Energy Environ. Sci.* **2012**, *5*, 9331–9344.
- (6) Strmcnik, D.; Uchimura, M.; Wang, C.; Subbaraman, R.; Danilovic, N.; van der Vliet, D.; Paulikas, A. P.; Stamenkovic, V. R.; Markovic, N. M. Improving the Hydrogen Oxidation Reaction Rate by Promotion of Hydroxyl Adsorption. *Nat. Chem.* **2013**, *5*, 300–306.
- (7) Kötz, E. R.; Stucki, S. Ruthenium Dioxide as a Hydrogen-Evolving Cathode. *J. Appl. Electrochem.* **1987**, *17*, 1190–1197.
- (8) Gasteiger, H. A.; Markovic, N.; Ross, P. N.; Cairns, E. J. Carbon Monoxide Electrooxidation on Well-Characterized Platinum–Ruthenium Alloys. *J. Phys. Chem.* **1994**, *98*, 617–625.
- (9) Hodnik, N.; Bele, M.; Hočvar, S. New Pt-Skin Electrocatalysts for Oxygen Reduction and Methanol Oxidation Reactions. *Electrochim. Commun.* **2012**, *23*, 125–128.
- (10) Watanabe, M.; Motoo, S. Electrocatalysis by Ad-Atoms: Part II. Enhancement of the Oxidation of Methanol on Platinum by Ruthenium Ad-Atoms. *J. Electroanal. Chem. Interfacial Electrochem.* **1975**, *60*, 267–273.
- (11) Iwasita, T. Electrocatalysis of Methanol Oxidation. *Electrochim. Acta* **2002**, *47*, 3663–3674.
- (12) Antolini, E. The Problem of Ru Dissolution from Pt–Ru Catalysts during Fuel Cell Operation: Analysis and Solutions. *J. Solid State Electrochem.* **2011**, *15*, 455–472.
- (13) Hsieh, Y.-C.; Zhang, Y.; Su, D.; Volkov, V.; Si, R.; Wu, L.; Zhu, Y.; An, W.; Liu, P.; He, P.; Ye, S.; Adzic, R. R.; Wang, J. X. Ordered Bilayer Ruthenium–Platinum Core–Shell Nanoparticles as Carbon Monoxide-Tolerant Fuel Cell Catalysts. *Nat. Commun.* **2013**, *4*, 1–8.
- (14) Abbott, D. F.; Mukerjee, S.; Petrykin, V.; Bastl, Z.; Halck, N. B.; Rossmeisl, J.; Krtík, P. Oxygen Reduction on Nanocrystalline Ruthenia—Local Structure Effects. *RSC Adv.* **2015**, *5*, 1235–1243.
- (15) Trasatti, S. Electrocatalysis in the Anodic Evolution of Oxygen and Chlorine. *Electrochim. Acta* **1984**, *29*, 1503–1512.
- (16) Daghetti, A.; Lodi, G.; Trasatti, S. Interfacial Properties of Oxides Used as Anodes in the Electrochemical Technology. *Mater. Chem. Phys.* **1983**, *8*, 1–90.
- (17) Kötz, R.; Lewerenz, H. J.; Stucki, S. XPS Studies of Oxygen Evolution on Ru and RuO₂ Anodes. *J. Electrochem. Soc.* **1983**, *130*, 825–829.
- (18) Wohlfahrt-Mehrens, M.; Heitbaum, J. Oxygen Evolution on Ru and RuO₂ Electrodes Studied Using Isotope Labelling and On-Line Mass Spectrometry. *J. Electroanal. Chem. Interfacial Electrochem.* **1987**, *237*, 251–260.
- (19) Jirkovský, J.; Makarova, M.; Krtík, P. Particle Size Dependence of Oxygen Evolution Reaction on Nanocrystalline RuO₂ and Ru_{0.8}Co_{0.2}O_{2-x}. *Electrochim. Commun.* **2006**, *8*, 1417–1422.
- (20) Zeradjanin, A. R.; Menzel, N.; Strasser, P.; Schuhmann, W. Role of Water in the Chlorine Evolution Reaction at RuO₂-Based Electrodes—Understanding Electrocatalysis as a Resonance Phenomenon. *ChemSusChem* **2012**, *5*, 1897–1904.
- (21) Reier, T.; Oezaslan, M.; Strasser, P. Electrocatalytic Oxygen Evolution Reaction (OER) on Ru, Ir, and Pt Catalysts: A Comparative Study of Nanoparticles and Bulk Materials. *ACS Catal.* **2012**, *2*, 1765–1772.
- (22) Lee, Y.; Suntivich, J.; May, K. J.; Perry, E. E.; Shao-Horn, Y. Synthesis and Activities of Rutile IrO₂ and RuO₂ Nanoparticles for Oxygen Evolution in Acid and Alkaline Solutions. *J. Phys. Chem. Lett.* **2012**, *3*, 399–404.
- (23) Cherevko, S.; Zeradjanin, A. R.; Topalov, A. A.; Kulyk, N.; Katsounaros, I.; Mayrhofer, K. J. J. Dissolution of Noble Metals during Oxygen Evolution in Acidic Media. *ChemCatChem* **2014**, *6*, 2219–2223.
- (24) Chang, S. H.; Danilovic, N.; Chang, K.-C.; Subbaraman, R.; Paulikas, A. P.; Fong, D. D.; Highland, M. J.; Baldo, P. M.; Stamenkovic, V. R.; Freeland, J. W.; Eastman, J. A.; Markovic, N. M. Functional Links between Stability and Reactivity of Strontium Ruthenate Single Crystals during Oxygen Evolution. *Nat. Commun.* **2014**, *5*, 1–9.
- (25) Danilovic, N.; Subbaraman, R.; Chang, K. C.; Chang, S. H.; Kang, Y.; Snyder, J.; Paulikas, A. P.; Strmcnik, D.; Kim, Y. T.; Myers, D.; Stamenkovic, V. R.; Markovic, N. M. Using Surface Segregation To Design Stable Ru-Ir Oxides for the Oxygen Evolution Reaction in Acidic Environments. *Angew. Chem., Int. Ed.* **2014**, *53*, 14016–14021.
- (26) Danilovic, N.; Subbaraman, R.; Chang, K. C.; Chang, S. H.; Kang, Y.; Snyder, J.; Paulikas, A. P.; Strmcnik, D.; Kim, Y. T.; Myers, D.; Stamenkovic, V. R.; Markovic, N. M. Activity–Stability Trends for the Oxygen Evolution Reaction on Monometallic Oxides in Acidic Environments. *J. Phys. Chem. Lett.* **2014**, *5*, 2474–2478.
- (27) Paoli, E. A.; Masini, F.; Frydendal, R.; Deiana, D.; Schlaup, C.; Malizia, M.; Hansen, T. W.; Horch, S.; Stephens, I. E. L.; Chorkendorff, I. Oxygen Evolution on Well-Characterized Mass-Selected Ru and RuO₂ Nanoparticles. *Chem. Sci.* **2015**, *6*, 190–196.
- (28) Frydendal, R.; Paoli, E. A.; Knudsen, B. P.; Wickman, B.; Malacrida, P.; Stephens, I. E. L.; Chorkendorff, I. Benchmarking the Stability of Oxygen Evolution Reaction Catalysts: The Importance of Monitoring Mass Losses. *ChemElectroChem.* **2014**, *1*, 2075–2081.
- (29) Fabbri, E.; Habereder, A.; Waltar, K.; Kotz, R.; Schmidt, T. J. Developments and Perspectives of Oxide-Based Catalysts for the Oxygen Evolution Reaction. *Catal. Sci. Technol.* **2014**, *4*, 3800–3821.
- (30) Zeradjanin, A. R.; Topalov, A. A.; Van Overmeire, Q.; Cherevko, S.; Chen, X.; Ventosa, E.; Schuhmann, W.; Mayrhofer, K. J. J. Rational Design of the Electrode Morphology for Oxygen Evolution—Enhancing the Performance for Catalytic Water Oxidation. *RSC Adv.* **2014**, *4*, 9579–9587.
- (31) Atanasoski, R.; Atanasoska, L.; Cullen, D.; Haugen, G.; More, K.; Vernstrom, G. Fuel Cells Catalyst for Start-Up and Shutdown Conditions: Electrochemical, XPS, and STEM Evaluation of Sputter-Deposited Ru, Ir, and Ti on Pt-Coated Nanostructured Thin Film Supports. *Electrocatalysis* **2012**, *3*, 284–297.
- (32) Pylypenko, S.; Blizanac, B. B.; Olson, T. S.; Konopka, D.; Atanassov, P. Composition- and Morphology-Dependent Corrosion Stability of Ruthenium Oxide Materials. *ACS Appl. Mater. Interfaces* **2009**, *1*, 604–611.
- (33) Zheng, J. P.; Cygan, P. J.; Jow, T. R. Hydrous Ruthenium Oxide as an Electrode Material for Electrochemical Capacitors. *J. Electrochem. Soc.* **1995**, *142*, 2699–2703.
- (34) Sopčić, S.; Roković, M. K.; Mandić, Z.; Róka, A.; Inzelt, G. Mass Changes Accompanying the Pseudocapacitance of Hydrous RuO₂ under Different Experimental Conditions. *Electrochim. Acta* **2011**, *56*, 3543–3548.
- (35) Sopčić, S.; Mandić, Z.; Roković, M. K. Some Factors Influencing Power and Energy Capabilities of RuO₂ Supercapacitors. *Acta Chim. Slov.* **2014**, *61*, 272–279.
- (36) Erjavec, B.; Dominko, R.; Umek, P.; Sturm, S.; Pejovnik, S.; Gaberscek, M.; Jamnik, J. RuO₂-Wired High-Rate Nanoparticulate TiO₂ (Anatase): Suppression of Particle Growth Using Silica. *Electrochim. Commun.* **2008**, *10*, 926–929.

- (37) Zhang, J.; Ma, J.; Zhang, L. L.; Guo, P.; Jiang, J.; Zhao, X. S. Template Synthesis of Tubular Ruthenium Oxides for Supercapacitor Applications. *J. Phys. Chem. C* **2010**, *114*, 13608–13613.
- (38) Allhusen, J. S.; Conboy, J. C. Preparation and Characterization of Conductive and Transparent Ruthenium Dioxide Sol–Gel Films. *ACS Appl. Mater. Interfaces* **2013**, *5*, 11683–11691.
- (39) Duonghong, D.; Borgarello, E.; Graetzel, M. Dynamics of Light-Induced Water Cleavage in Colloidal Systems. *J. Am. Chem. Soc.* **1981**, *103*, 4685–4690.
- (40) Bratsch, S. G. Standard Electrode Potentials and Temperature Coefficients in Water at 298.15 K. *J. Phys. Chem. Ref. Data* **1989**, *18*, 1–21.
- (41) Chang, S. H.; Connell, J. G.; Danilovic, N.; Subbaraman, R.; Chang, K.-C.; Stamenkovic, V. R.; Markovic, N. M. Activity–Stability Relationship in the Surface Electrochemistry of the Oxygen Evolution Reaction. *Farad. Discuss.* **2014**, *176*, 125–133.
- (42) Jovanović, P.; Pavlišić, A.; Šelih, V. S.; Šala, M.; Hodnik, N.; Bele, M.; Hočevar, S.; Gaberšček, M. New Insight into Platinum Dissolution from Nanoparticulate Platinum-Based Electrocatalysts Using Highly Sensitive in Situ Concentration Measurements. *ChemCatChem* **2014**, *6*, 449–453.
- (43) Pavlisic, A.; Jovanovic, P.; Selih, V. S.; Sala, M.; Hodnik, N.; Hocevar, S.; Gaberscek, M. The Influence of Chloride Impurities on Pt/C Fuel Cell Catalyst Corrosion. *Chem. Commun.* **2014**, *50*, 3732–3734.
- (44) Hodnik, N.; Zorko, M.; Bele, M.; Hočevar, S.; Gaberšček, M. Identical Location Scanning Electron Microscopy: A Case Study of Electrochemical Degradation of PtNi Nanoparticles Using a New Nondestructive Method. *J. Phys. Chem. C* **2012**, *116*, 21326–21333.
- (45) Zorko, M.; Jozinović, B.; Bele, M.; Hodnik, N.; Gaberšček, M. SEM Method for Direct Visual Tracking of Nanoscale Morphological Changes of Platinum Based Electrocatalysts on Fixed Locations upon Electrochemical or Thermal Treatments. *Ultramicroscopy* **2014**, *140*, 44–50.
- (46) Cherevko, S.; Zeradjanin, A. R.; Keeley, G. P.; Mayrhofer, K. J. J. A Comparative Study on Gold and Platinum Dissolution in Acidic and Alkaline Media. *J. Electrochem. Soc.* **2014**, *161*, H822–H830.
- (47) Topalov, A. A.; Cherevko, S.; Zeradjanin, A. R.; Meier, J. C.; Katsounaras, I.; Mayrhofer, K. J. J. Towards a Comprehensive Understanding of Platinum Dissolution in Acidic Media. *Chemical Science* **2014**, *5*, 631–638.
- (48) Pourbaix, M. *Atlas of Electrochemical Equilibria in Aqueous Solutions*; Pergamon Press: New York, 1966.
- (49) Herd, B.; Goritzka, J. C.; Over, H. Room Temperature Oxidation of Ruthenium. *J. Phys. Chem. C* **2013**, *117*, 15148–15154.
- (50) Ardizzone, S.; Fregonara, G.; Trasatti, S. “Inner” and “Outer” Active Surface of RuO₂ Electrodes. *Electrochim. Acta* **1990**, *35*, 263–267.
- (51) Zeng, K.; Zhang, D. Recent Progress in Alkaline Water Electrolysis for Hydrogen Production and Applications. *Prog. Energy Combust.* **2010**, *36*, 307–326.
- (52) Cherevko, S.; Reier, T.; Zeradjanin, A. R.; Pawolek, Z.; Strasser, P.; Mayrhofer, K. J. J. Stability of Nanostructured Iridium Oxide Electrocatalysts during Oxygen Evolution Reaction in Acidic Environment. *Electrochim. Commun.* **2014**, *48*, 81–85.